Extended and knotted optical traps in three dimensions

Elisabeth R. Shanblatt and David G. Grier
Department of Physics and Center for Soft Matter Research, New York University, New York, NY 10003

Abstract: We describe a method for projecting holographic optical traps that are extended along arbitrary curves in three dimensions, and whose amplitude and phase profiles are specified independently. This approach can be used to create bright optical traps with knotted optical force fields.

OCIS codes: (090.1760) Computer holography; (140.7010) Laser trapping

References and links

1. Y. Roichman and D. G. Grier, "Projecting extended optical traps with shape-phase holography," Opt. Lett. **31**, 1675–1677 (2006).
2. Y. Roichman and D. G. Grier, "Three-dimensional holographic ring traps," Proc. SPIE **6483**, 64830F (2007).
3. Y. Roichman, B. Sun, Y. Roichman, J. Amato-Grill, and D. G. Grier, "Optical forces arising from phase gradients," Phys. Rev. Lett. **100**, 013602 (2008).
4. S.-H. Lee, Y. Roichman, and D. G. Grier, "Optical solenoid beams," Opt. Express **18**, 6988–6993 (2010).
5. A. Ashkin, J. M. Dziedzic, J. E. Bjorkholm, and S. Chu, "Observation of a single-beam gradient force optical trap for dielectric particles," Opt. Lett. **11**, 288–290 (1986).
6. H. He, N. R. Heckenberg, and H. Rubinsztein-Dunlop, "Optical particle trapping with higher-order doughnut beams produced using high efficiency computer generated holograms," J. Mod. Opt. **42**, 217–223 (1995).
7. N. B. Simpson, L. Allen, and M. J. Padgett, "Optical tweezers and optical spanners with Laguerre-Gaussian modes," J. Mod. Opt. **43**, 2485–2491 (1996).
8. K. T. Gahagan and G. A. Swartzlander, "Optical vortex trapping of particles," Opt. Lett. **21**, 827–829 (1996).
9. K. Ladavac and D. G. Grier, "Microoptomechanical pump assembled and driven by holographic optical vortex arrays," Opt. Express **12**, 1144–1149 (2004).
10. K. Ladavac and D. G. Grier, "Colloidal hydrodynamic coupling in concentric optical vortices," Europhys. Lett. **70**, 548–554 (2005).
11. H. He, M. E. J. Friese, N. R. Heckenberg, and H. Rubinsztein-Dunlop, "Direct observation of transfer of angular momentum to absorptive particles from a laser beam with a phase singularity," Phys. Rev. Lett. **75**, 826–829 (1995).
12. J. W. Goodman, *Introduction to Fourier Optics*, 3rd ed. (McGraw-Hill, New York, 2005).
13. G. C. Sherman, "Application of the convolution theorem to Rayleigh's integral formulas," J. Opt. Soc. Am. **57**, 546–547 (1967).
14. M. Reicherter, T. Haist, E. U. Wagemann, and H. J. Tiziani, "Optical particle trapping with computer-generated holograms written on a liquid-crystal display," Opt. Lett. **24**, 608–610 (1999).
15. J. Liesener, M. Reicherter, T. Haist, and H. J. Tiziani, "Multi-functional optical tweezers using computer-generated holograms," Opt. Commun. **185**, 77–82 (2000).
16. J. E. Curtis, B. A. Koss, and D. G. Grier, "Dynamic holographic optical tweezers," Opt. Commun. **207**, 169–175 (2002).
17. J. Leach, K. Wulff, G. Sinclair, P. Jordan, J. Courial, L. Thomson, G. Gibson, K. Karunwi, Z. J. Cooper, John an dLaczik, and M. Padgett, "Interactive approach to optical tweezers control," Appl. Opt. **45**, 897–903 (2006).
18. Y. Roichman, I. Cholis, and D. G. Grier, "Volumetric imaging of holographic optical traps," Opt. Express **14**, 10,907–10,912 (2006).
19. M. Polin, K. Ladavac, S.-H. Lee, Y. Roichman, and D. G. Grier, "Optimized holographic optical traps," Opt. Express **13**, 5831–5845 (2005).
20. J. C. Crocker and D. G. Grier, "Methods of digital video microscopy for colloidal studies," J. Colloid Interface Sci. **179**, 298–310 (1996).
21. L. Allen, M. W. Beijersbergen, R. J. C. Spreeuw, and J. P. Woerdman, "Orbital angular-momentum of light and the transformation of Laguerre-Gaussian laser modes," Phys. Rev. A **45**, 8185–8189 (1992).

22. A. T. O'Neil, I. MacVicar, L. Allen, and M. J. Padgett, "Intrinsic and extrinsic nature of the orbital angular momentum of a light beam," Phys. Rev. Lett. **88**, 053601 (2002).
23. J. E. Curtis and D. G. Grier, "Structure of optical vortices," Phys. Rev. Lett. **90**, 133901 (2003).
24. S. Sundbeck, I. Gruzberg, and D. G. Grier, "Structure and scaling of helical modes of light," Opt. Lett. **30**, 477–479 (2005).
25. J. Leach, M. R. Dennis, J. Courtial, and M. J. Padgett, "Knotted threads of darkness," Nature **432**, 165 (2004).
26. M. R. Dennis, R. P. King, J. Barry, K. O'Holleran, and J. Padgett, Miles, "Isolated optical vortex knots," Nature Phys. **6**, 53–56 (2010).
27. W. T. M. Irvine and D. Bouwmeester, "Linked and knotted beams of light," Nature Phys. **4**, 716–720 (2008).
28. L. Faddeev and A. J. Niemi, "Stable knot-like structures in classical field theory," Nature **387**, 58–61 (1997).

Extended optical traps are structured light fields whose intensity and phase gradients exert forces that confine microscopic objects to one-dimensional curves in three dimensions [1, 2, 3, 4]. Intensity-gradient forces typically are responsible for trapping [5] in the two transverse directions, while radiation pressure directed by phase gradients can move particles along the third [3, 4]. This combination of trapping and driving has been demonstrated dramatically in optical vortexes [6, 7, 8, 9, 10], ring-like optical traps that are created by focusing helical modes of light. Intensity gradients draw illuminated objects toward the ring, and phase gradients then drive them around [3, 7, 8, 11]. More recently, holographic methods have been introduced to design and project more general optical traps that are extended along lines [1], rings [2] and helices [4], with intensity and phase profiles independently specified along their lengths. Unlike optical vortexes, these traps feature nearly ideal axial intensity gradients because they are specifically designed to achieve diffraction-limited focusing [1, 2, 3, 4].

Here, we describe a method for designing and projecting optical traps whose intensity maxima trace out more general curves in three dimensions with independently specified phase and amplitude profiles. Within limitations set by Maxwell's equations, these three-dimensional light fields can be used to trap and move microscopic objects. We demonstrate the technique by projecting diffraction-limited holographic ring traps with arbitrary orientations in three dimensions.

More specifically, our goal is to project a beam of light that comes to a focus along a curve $\vec{R}_0(s) = (x_0(s), y_0(s), z_0(s))$, parametrized by its arc length s, along which the amplitude $a_0(s)$ and phase $\varphi_0(s)$ also are specified. The three-dimensional light field $u(\vec{r},z)$ embodying this extended optical trap is projected by a lens of focal length f, and so passes through the lens' focal plane where its value is $u_f(\vec{r},0) = u_f(\vec{r})$. Associated with $u_f(\vec{r})$ is the conjugate field $u_h(\vec{r})$ in the back focal plane of the lens, over which we have control. A hologram that imprints this field onto the wavefronts of an otherwise featureless laser beam will project the desired trapping pattern $u(\vec{r},z)$ downstream of the lens, as illustrated in Fig. 1.

The ideal hologram, $u_h(\vec{\rho}) = a_h(\vec{\rho}) \exp(i\varphi_h(\vec{\rho}))$, is characterized by a real-valued amplitude $a_h(\vec{\rho})$ and phase $\varphi_h(\vec{\rho})$ both of which vary with position $\vec{\rho} = (\xi, \eta)$ in the back focal plane. It is related to the projected field, $u_f(\vec{r})$, by a Fresnel transform [12]

$$u_h(\vec{\rho}) = \frac{k}{2\pi i} \int_\Omega u_f(\vec{r}) \exp\left(i \frac{k}{f} \vec{r} \cdot \vec{\rho} \right) d^2 r, \tag{1}$$

where $k = 2\pi n_m/\lambda$ is the wavenumber of light of vacuum wavelength λ in a medium of refractive index n_m, and where Ω is the effective aperture of the optical train. In the limit that the aperture is large, $u_h(\vec{\rho})$ is related to the Fourier transform, $\tilde{u}_f(\vec{q})$, of $u_f(\vec{r})$ by

$$u_h(\vec{\rho}) = -\frac{i}{\lambda} \tilde{u}_f(\vec{q}) \tag{2}$$

with $\vec{q} = k\vec{\rho}/f$.

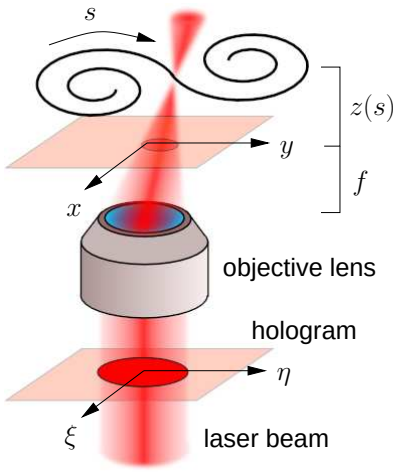

Fig. 1. Projecting three-dimensionally extended holographic traps. A laser beam is imprinted with a hologram in the input pupil of an objective lens. The hologram is projected through the objective's focal plane, and comes to a focus along a three-dimensional curve parameterized by its arc length, s.

For extended traps that lie entirely within the focal plane, the projected field may be approximated by an infinitessimally fine thread of light $u_f(\vec{r}) \approx a_0(s)\exp(i\varphi_0(s))\,\delta(\vec{r}-\vec{r}_0(s))$, where $\vec{r}_0(s) = (x_0(s), y_0(s))$ [1, 2, 3]. Equation (2) then yields a hologram associated with this idealized design. The projected field comes to a focus of finite width because Eq. (2) naturally incorporates contributions from self-diffraction.

Extending this to more general three-dimensional curves poses challenges that have been incompletely addressed in previous studies [4]. The field $u(\vec{r},z)$ at height z above the focal plane is related to the field in the focal plane by the Rayleigh-Sommerfeld diffraction integral [12], which is expressed conveniently with the Fourier convolution theorem as

$$u(\vec{r},z) = \exp(-ikz)\int H_z(\vec{q})\,\tilde{u}_f(\vec{q})\exp(i\vec{q}\cdot\vec{r})\,d^2q, \tag{3}$$

where

$$H_z(\vec{q}) = \exp\left(iz\left(k^2-q^2\right)^{1/2}\right) \tag{4}$$

is the Fourier transform of the Rayleigh-Sommerfeld propagator [13]. Ideally, $u_f(\vec{r})$ would be associated with a three-dimensional field $u(\vec{r},z)$ that satisfies $u(\vec{r}_0(s), z_0(s)) = a(s)\exp(i\varphi(s))$. Equation (3), however, is not simply invertible unless $u(\vec{r},z)$ is completely specified on a single plane, z. In the absence of such a comprehensive description, we introduce the approximation

$$\tilde{u}_f(\vec{q}) \approx \int a_0(s)\exp(-\varphi_0(s))\exp(ikz_0(s))\,H_{-z_0(s)}(\vec{q})\exp(-i\vec{q}\cdot\vec{r}_0(s))\,ds \tag{5}$$

that arises from simple superposition of contributions from each element of the curve. Equation (5) is not an inversion of Eq. (3) because it neglects light propagating from one region of $\vec{R}_0(s)$ interfering with light elsewhere along the curve. In this sense, it resembles the "gratings and lenses" algorithm developed for projecting point-like optical traps [14, 15, 16, 17], which also fails to account for cross-talk. The Rayleigh-Sommerfeld propagator improves upon the simpler parabolic phase profiles used for axial displacements in these earlier studies.

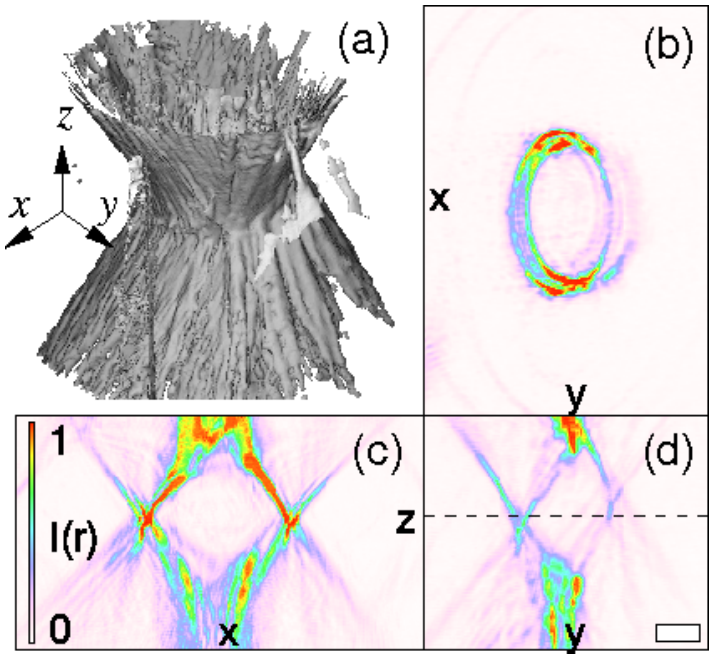

Fig. 2. (a) Volumetric reconstruction of a tilted ring trap. (b) Horizontal section near the midplane showing tilt around the $\hat{y}$ axis. (c) Vertical section along the $\hat{x}$ axis. (d) Vertical section along the $\hat{y}$ axis.

As an application of Eq. (5), we create a uniformly bright ring trap [2] of radius R, rotated by angle β about the $\hat{y}$ axis. The trap's focus follows the curve

$$\vec{R}_0(s) = R\left(\cos\left(\frac{s}{R}\right)\cos\beta, \sin\left(\frac{s}{R}\right), \cos\left(\frac{s}{R}\right)\sin\beta\right), \tag{6}$$

with the arc length ranging from $s = 0$ to $s = 2\pi R$. Equations (2) and (5) then yield the hologram

$$u_h(\vec{\rho}) = J_0\left(A(\vec{\rho})\right) \tag{7}$$

up to arbitrary phase factors, where $J_0(.)$ is the Bessel function of the first kind of order zero and $A(\vec{\rho})$ satisfies

$$\left(\frac{2fA(\vec{\rho})}{kR}\right)^2 = \xi^2 + \left[\eta\cos\beta + \left(4f^2+\rho^2\right)^{1/2}\sin\beta\right]^2. \tag{8}$$

This reduces to

$$u_h(\vec{\rho}) = J_0\left(\frac{kR}{2f}\rho\right) \tag{9}$$

when $\beta = 0$, which is the previously reported result for a holographic ring trap aligned with the focal plane [2].

Figure 2(a) is a volumetric reconstruction [18] of the three-dimensional intensity distribution projected by the hologram in Eq. (7) of a ring trap of radius $R = 9$ μm tilted at $\beta = \pi/4$ rad. This complex-valued hologram was approximated with a phase-only hologram using the shape-phase algorithm [1] so that it could be projected with a conventional holographic optical trapping system [19]. The light from a diode-pumped solid-state laser (Coherent Verdi,

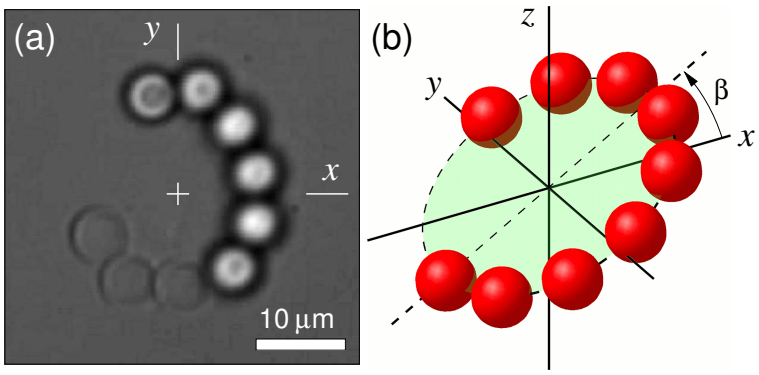

Fig. 3. (a) Bright-field microscope image of 5.17 μm diameter colloidal silica spheres trapped on an inclined ring. (b) Schematic representation of the geometry in (a). The Media file shows particles circulating around the inclined ring under the influence of phase-gradient forces.

$\lambda = 532$ nm) was imprinted with the computed hologram by a phase-only liquid-crystal spatial light modulator (Hamamatsu X8267-16 PPM) and relayed to the input pupil of an oil-immersion objective lens (Nikon Plan-Apo, 100×, numerical aperture 1.4) mounted in a conventional light microscope (Nikon TE-2000U). Transverse slices of the projected intensity distribution, such as the example in Fig. 2(b), were obtained by mounting a front-surface mirror on the microscope's sample stage and moving the trap with respect to the focal plane. Light reflected by the mirror was collected by the same objective lens and relayed to a video camera (NEC TI-324A II) for recording. A sequence of such slices obtained in axial steps of $\Delta z = 0.1$ μm was stacked to create a volumetric map of the trap's intensity. The surface in Fig. 2(a) encompasses the brightest 70 percent of the pixels in each slice. The axial sections through the volume in Figs. 2(c) and (d) confirm the inclination of the ring.

Figure 3 shows a typical bright-field image of 5.17 μm diameter silica spheres dispersed in water and trapped on the inclined ring. A sphere's appearance varies from bright to dark depending on its axial distance from the microscope's focal plane. This dependence can be calibrated to estimate the sphere's axial position [20]. The image in Fig. 3 is consistent with the designed inclination of the ring trap and therefore demonstrates the efficacy of Eqs. (2) and (5) for designing three-dimensionally extended optical traps.

In addition to extending an optical trap's intensity along a three-dimensional curve, Eq. (5) also can be used to specify the extended trap's phase profile. Imposing a uniform phase gradient, $\varphi_\ell(s) = \ell(s/R)$, redirects the light's momentum flux to create a uniform phase-gradient force [3] directed along the trap. In the particular case of a ring trap, this additional tangential force may be ascribed to orbital angular momentum in the beam [21] that is independent of the light's state of polarization [22] and makes trapped particles circulate around the ring [2, 3, 11]. This principle can be applied also to inclined ring traps.

Unlike a horizontal ring trap [2] at $\beta = 0$, the inclined ring inevitably has phase variations along its circumference, $\varphi(s) = kz(s)$, whose azimuthal gradient $\partial_s \varphi(s) = -k\sin(s/R)\sin\beta$ tends to drive trapped objects to the downstream end of the ring [3]. Adding $\varphi_\ell(s)$ to this intrinsic phase profile creates a tilted ring trap described by the hologram

$$u_h(\vec{\rho}) = J_\ell(A(\vec{\rho}))\exp\left(2\pi i\ell\frac{s}{R}\right) \tag{10}$$

whose additional circumferential phase gradient that tends to drive particles around the ring. Here, $J_\ell(.)$ is the Bessel function of the first kind of order ℓ. A particle should circulate contin-

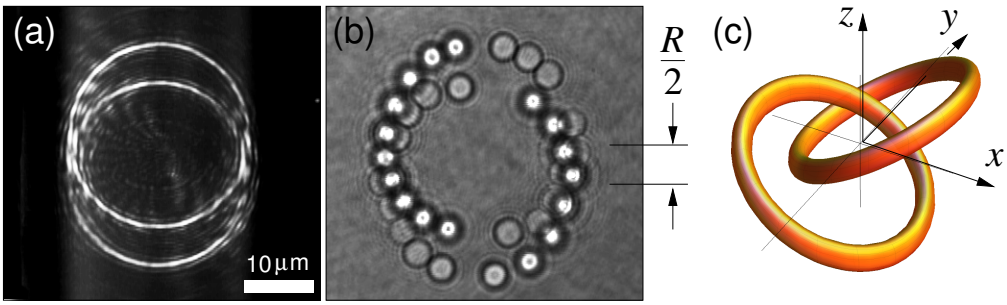

Fig. 4. (a) Intensity in the focal plane of the microscope of two tilted ring traps projected simultaneously with opposite inclination, $\beta = \pm\pi/8$. (b) Colloidal silica spheres trapped in three dimensions within the focused Hopf link. (c) Schematic representation of the three-dimensional intensity distribution responsible for the image in (a).

uously if this tangential gradient is large enough to overcome the overall downstream gradient, which occurs for $\ell > n_m (R/\lambda) sin\beta$. Diffraction limits the maximum value of ℓ [2, 23, 24] that can be imposed on a ring trap of radius R. This, in turn, limits the maximum tilt angle β for which free circulation is possible.

The images in Fig. 3 were obtained with no imposed phase gradient, $\ell = 0$. Increasing ℓ to 20 directs enough of the beam's radiation pressure in the tangential direction to drive the spheres around the ring at roughly 0.2 Hz. Colloidal spheres can be seen circulating around an inclined ring trap in the Media file associated with Fig. 3.

The same formalism can be used to make more complicated three-dimensional trapping fields. The image in Fig. 4(a) shows the intensity in the focal plan of two tilted ring traps of radius $R = 12.9$ μm projected simultaneously but with opposite inclination, $\beta = \pm\pi/8$. Setting these rings' separation to $R/2$ creates a pair of interlocking bright rings in the form of a Hopf link. These interpenetrating rings still act as three-dimensional optical traps, and are shown in Fig. 4(b) organizing 3.01 μm diameter colloidal silica spheres. The trapped spheres pass freely past each other along the two rings. Figure 4(c) offers a schematic view of the Hopf link geometry.

This knotted light field differs from previously reported knotted vortex fields [25, 26] in that its intensity is maximal along the knot, rather than minimal. In this respect, holographically projected Hopf links more closely resemble the Ranada-Hopf knotted fields that have been predicted [27] for strongly focused circularly polarized optical pulses. Knotted force fields arise in this latter case from knots in each pulse's magnetic field. Linked ring traps are not knotted in this sense. Nevertheless, the programmable combination of intensity-gradient and phase-gradient forces in linked ring traps can create a constant knotted force field for microscopic objects. Beyond their intrinsic interest, such knotted optical force fields have potential applications in plasma physics for inducing knotted current loops [27, 28] and could serve as mixers for biological and soft-matter systems at the micrometer scale.

This work was supported by the MRSEC Program of the National Science Foundation through Grant Number DMR-0820341.